

Aligned Disentangling GAN: A Leap towards End-to-end Unsupervised Nuclei Segmentation

Kai Yao

Xi'an Jiaotong-Liverpool University
Suzhou, Jiangsu Province, China
kai.yao19@student.xjtlu.edu.cn

Jie Sun

Xi'an Jiaotong-Liverpool University
Suzhou, Jiangsu Province, China

Kaizhu Huang

Xi'an Jiaotong-Liverpool University
Suzhou, Jiangsu Province, China
kaizhu.huangh@student.xjtlu.edu.cn

Curran Jude

University of Liverpool

Abstract

We consider unsupervised cell nuclei segmentation in this paper. Exploiting the recently-proposed unpaired image-to-image translation between cell nuclei images and randomly synthetic masks, existing approaches, e.g. CycleGAN, have achieved encouraging results. However, these methods usually take a two-stage pipeline and fail to learn end-to-end in cell nuclei images. More seriously, they could lead to the lossy transformation problem, i.e., the content inconsistency between the original images and the corresponding segmentation output. To address these limitations, we propose a novel end-to-end unsupervised framework called Aligned Disentangling Generative Adversarial Network (AD-GAN). Distinctively, AD-GAN introduces representation disentanglement to separate content representation (the underling spatial structure) from style representation (the rendering of the structure). With this framework, spatial structure can be preserved explicitly, enabling a significant reduction of macro-level lossy transformation. We also propose a novel training algorithm able to align the disentangled content in the latent space to reduce micro-level lossy transformation. Evaluations on real-world 2D and 3D datasets show that AD-GAN substantially outperforms the other comparison methods and the professional software both quantitatively and qualitatively. Specifically, the proposed AD-GAN leads to significant improvement over the current best unsupervised methods by an average 17.8% relatively (w.r.t. the metric DICE) on four cell nuclei datasets. As an unsupervised method, AD-GAN even performs competitive with the best supervised models, taking a further leap towards end-to-end unsupervised nuclei

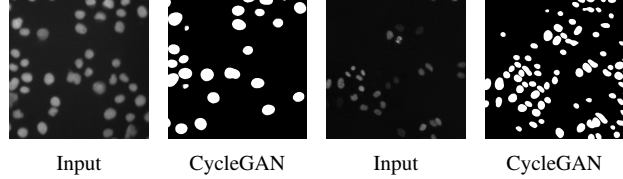


Figure 1. Examples of the lossy transformation problem.

segmentation.¹

1. Introduction

Fluorescence microscopy image analysis, particularly automatic cell nuclei image segmentation, is essential for quantifying cell models efficiently and accurately. Supervised nuclei segmentation methods have achieved impressive results on fluorescence microscope images [9]. However, due to variations of settings, annotation noises, and/or insufficient labelled data, these methods are usually difficult to be used in practice. For this reason, recent research focus has shifted to unsupervised nuclei segmentation.

The objective of unsupervised nuclei segmentation is to obtain the segmentation mask accurately via a one-to-one mapping from the input nuclei image without any annotation information. This problem can also be considered as unpaired image-to-image translation, meaning that no pair ground-truth is available between the nuclei image and the segmentation mask. Recent studies show that CycleGAN based unsupervised nuclei segmentation achieves the current state-of-the-art results. For instance, Bohland *et al.* investigated in a systematic study about the influence of synthetic masks' object properties on CycleGAN supported

¹Source codes of AD-GAN can be found in the supplementary material.

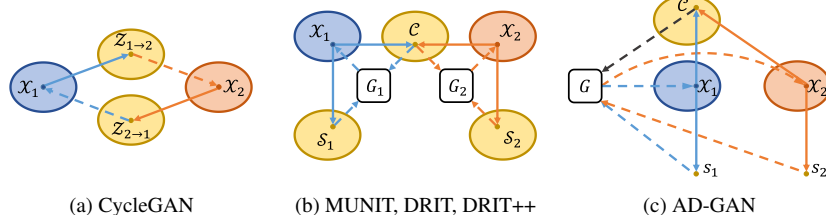


Figure 2. Comparisons of unsupervised image-to-image translation models. Denote x_1 and x_2 as images in domain \mathcal{X}_1 and \mathcal{X}_2 : (a) CycleGAN maps x_1 and x_2 onto separated latent spaces. (b) Common representation disentangling models disentangle the latent spaces of x_1 and x_2 into a shared content space \mathcal{C} and a separate style space \mathcal{S} for each domain. (c) In our AD-GAN, one single style is assumed for each domain (which holds in nuclei cell image segmentation). AD-GAN can disentangle the latent spaces of x_1 and x_2 into a shared content space \mathcal{C} and two single domain style representation s_1 and s_2 . AD-GAN enjoys a more simple, accurate, and end-to-end structure.

segmentation pipelines [2]. They first trained a CycleGAN to create paired synthetic data from the synthetic masks, and then learned a semantic segmentation model. Fu *et al.* developed a spatial constrained CycleGAN (SpCycleGAN) [10] to deal with the spatial offset problem in 3D images and then used synthetic paired dataset on supported 3D segmentation pipelines [8].

Despite their success, these CycleGAN based methods are usually not trained end-to-end when used in nuclei cell segmentation, since they need generate firstly synthetic data so as to form the paired data. More seriously, the so-called lossy transformation problem [5] usually exists, i.e., the content inconsistency between the original images and the corresponding segmentation (mask) output. Such inconsistency includes nuclei deletion/addition at the macro-level, and location offset, shape difference at the micro-level, which can be seen in Fig. 1. Though some recent methods [10, 31, 24] have been proposed attempting to alleviate it by adding regularization terms or matching the exact global properties, their performance is still limited. Particularly, these recent frameworks all engage entangled representation models [32], making them difficult to separate the content (semantic parts to be segmented) from the style (semantic parts to be masked or removed).

In this work, we propose a novel end-to-end framework, called Aligned Disentangling Generative Adversarial Network (AD-GAN) to address the lossy transformation problem typically in unsupervised nuclei segmentation. Inspired by recent achievements on image-to-image translation [14, 21, 22], we take advantages of representation disentanglement and exploit the auto-encoder as the generator to extract disentangled representations. Different from the existing general-purpose representation disentangling models which learn distinctive style for each sample, we assume that a single domain style can be learned for either the nuclei image domain or the synthetic mask domain, which holds for most nuclei images and synthetic segmentation masks since they all contain very simple textures (see Fig. 1). We also design a unified framework able to take one-hot do-

main labels to control translation directions. With this novel design, the disentangled content representation of the two domains can share the same latent space naturally. We further propose an aligned disentangling training strategy, capable of aligning the disentangled content representation in the latent space. The aligned content representation ensures one-to-one mapping not only at the image level but also at the semantic object level. Importantly, evaluations on 2D and 3D datasets show our method can substantially alleviate the lossy transformation problem and achieve significant improvements over the current best CycleGAN based methods.

Overall, the contributions of this paper are fourfold: (i) we propose a novel end-to-end unsupervised nuclei segmentation framework called AD-GAN. We take a further leap and achieve so far the best results with an improvement of 17.8% averagely on both 2D and 3D data (even comparable with those of supervised methods); (ii) we alleviate the macro-level lossy transformation problem in unsupervised nuclei segmentation by learning disentangled representations with a much simple yet effective architecture; (iii) we propose a novel training strategy called Aligned Disentangling Training which can further align the disentangled content representation to reduce micro-level lossy transformation problem; (iv) by better coping with the lossy transformation problem, our proposed method can be readily extended to instance segmentation and image synthesis.

2. Related Work

Existing unsupervised nuclei segmentation methods [11, 3, 12, 10, 2] usually adopt a two-stage pipeline, i.e., 1) they first generate synthetic data so as to pair the input images and the synthetic masks, and 2) they learn the segmentation model with the synthetic paired data. Able to exploit the cycle consistency to ensure a good bidirectional mapping as depicted in Fig. 2(a), CycleGAN and its variants are typically used in the first stage. On one hand, these methods cannot be trained end-to-end, making it difficult to be applied in practice. On the other hand, the lossy trans-

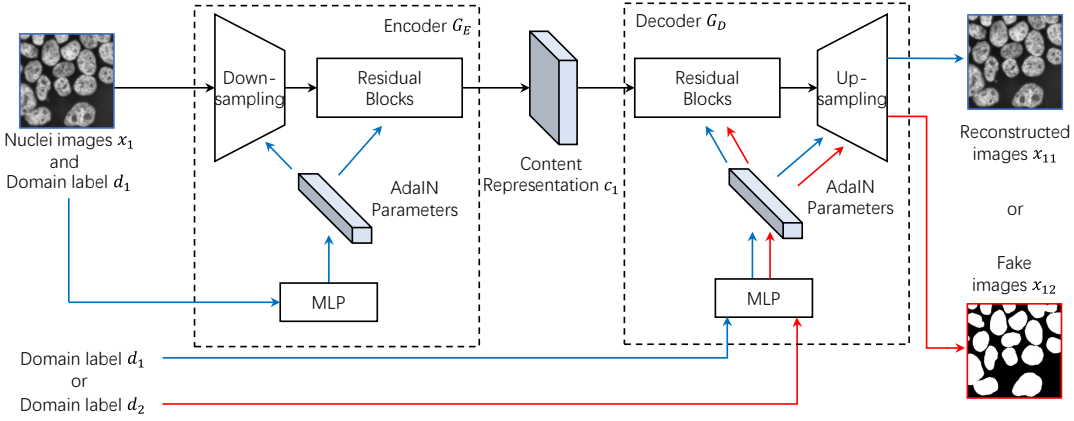


Figure 3. Architecture of the proposed auto-encoder based generator. Under our within-domain same-style assumption in this task, the major style of each domain can be learned as style representation so that the disentangled content can be preserved explicitly.

formation problem commonly exists in these methods. To alleviate this drawback, SpCycleGAN [10] was proposed with a spatial regularization term for avoiding the spatial offset problem; UDCT [31] was also developed by adding a novel histogram discriminator to make the style transfer more reliable. Though some encouraging results have been achieved, these methods do not learn disentangled representations. Consequently they cannot well separate the contents from the styles and fail to handle the lossy transformation problem appropriately.

Aiming to decompose contents and style explicitly, recent studies focused on learning disentangled representations [14, 1, 21, 22]. By assuming that the domain-invariant representation refers to content and the domain-specific representation refers to style, these methods have obtained substantial improvement in general-purpose unpaired image-to-image translation. Unfortunately, when applied in unsupervised nuclei segmentation, these methods may not achieve satisfactory performance. In particular, they assume that the style is diverse within domain and learn distinctive style for each sample, as illustrated in Fig. 2(b). However, nuclei cell images typically contains simple style in both image domain and the mask domain. In this scenario, given too flexible styles, contents (or nuclei objects) may not necessarily be represented by domain-invariant features; instead, some contents may be described by certain domain-specific features. Therefore, some contents (nuclei) could be incorrectly learned as styles and are then removed in the mask domain, resulting in the content inconsistency during cross-domain translation.

Different from the above mentioned methods, we assume one single style can be learned for each domain, as consistently observed from the nuclei images and synthetic masks. This enables an efficient and simple disentanglement framework. Separating content from style efficiently, our pro-

posed framework can not only be trained end-to-end, but also achieves remarkably better performance than the previous methods including the current popular professional software for unsupervised nuclei segmentation. It is noticed that, UFDN [23] has a similar assumption to ours that each domain has one domain style. They use VAE to disentangle content feature and it is not guaranteed that the features are fully disentangled due to lack of cycle consistency [28].

3. Proposed Method

We solve the unsupervised nuclei segmentation as an unsupervised unpaired image-to-image translation problem in this paper. Two different domain images are considered, i.e. the microscope cell image domain \mathcal{X}_1 and the synthetic segmentation mask domain \mathcal{X}_2 , which can be easily generated by inserting 2D ellipse or 3D ellipsoid structure with random rotations and translations.

We propose a novel GAN-based model termed as AD-GAN as illustrated in Fig. 2(c). Specifically, we design a novel framework to disentangle the latent spaces of images and masks into a shared content space \mathcal{C} and two single style representations, one for each domain. With the same-style assumption within each domain, a disentanglement of content from styles can be efficiently accomplished by conditioning domain labels. This also enables us to design a novel unified single generator in contrast to two generators as typically required in the traditional disentanglement models (see Fig. 2(b) and 2(c)). With a novel training strategy called Aligned Disentangling Training, the proposed framework can not only be trained end-to-end, but also it can ensure that the disentangled content representation of the two domains are readily aligned and mapped to the same latent space.

In the following, we will first focus on introducing the

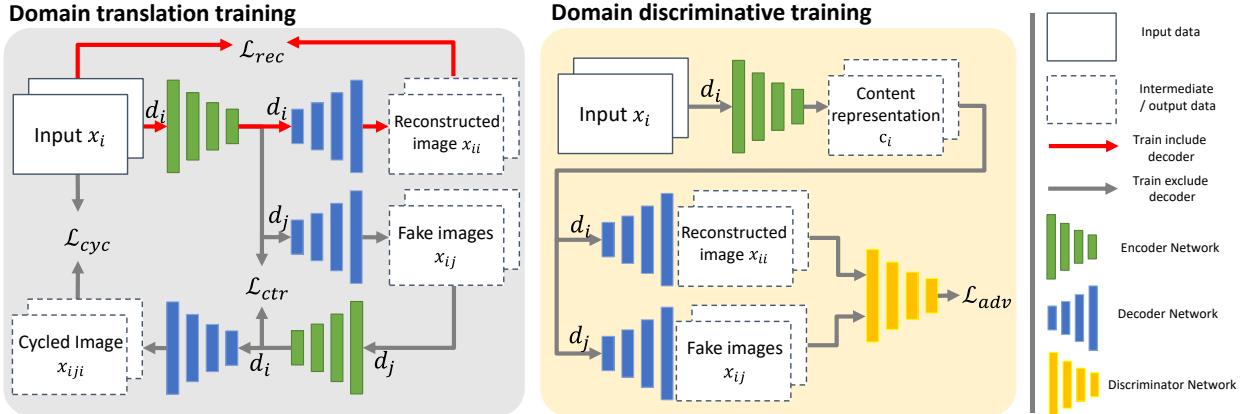


Figure 4. Overview of the training scheme in AD-GAN. The grey block shows the within- and cross-domain translation component for Image x_i in domain \mathcal{X}_i , while the orange block indicates our domain discriminative training component. d_i ($i \in \{1, 2\}$) denotes the domain label controlling the translation direction.

novel unified generator G of AD-GAN while exploiting a domain discriminator [4] in our design which is a standard Markovian discriminator [16] with two output branches. We then discuss how we design the novel aligned disentangling training as well as the theoretical interpretation of our method. Finally, we describe the loss function for optimizing the whole GAN network.

3.1. Architecture of Generator

Let $x_i \in \mathcal{X}_i$ ($i = 1, 2$) represent a sample from the cell image domain or synthetic mask domain, and d_i denote the corresponding domain label. Fig. 3 shows the architecture of our auto-encoder based generator G , which consists of an encoder G_E and a decoder G_D . Different with MUNIT [14] which uses a style encoder to extract diverse style code, we use the domain label to replace the style code, so that one single style representation for each domain can be learned by a multi-layer perceptron (MLP). Inspired by recent work that uses affine transformation parameters in normalization layers to represent styles [14, 4], we equip both the encoder and decoder with Adaptive Instance Normalization (AdaIN) [13] layers to inject the style representations. Moreover, we use a unified framework for both domains since the two learned style representations are discriminative. As shown in the blue path of Fig. 3 a content representation c_i can be factorized by the encoder conditioned on domain label d_i , which reflects the nature of nuclei images and masks in this task i.e., $c_i = G_E(x_i, d_i)$. Simultaneously, the content representation c_i and the style representation learned from domain label d_i can be composed into reconstructed image x_{ii} by the decoder, e.g., $x_{ii} = G_D(G_E(x_i, d_i), d_i)$. Image-to-image translation is performed by swapping decoder's domain label to another, as illustrated in the red path of Fig. 3. Consequently, fake images x_{ij} can be obtained, e.g.,

$$x_{ij} = G_D(G_E(x_i, d_i), d_j), i \neq j.$$

In addition, we adapt a domain discriminator [4] in our design which is a standard Markovian discriminator [16] with two output branches. Each branch D_i learns a binary classification determining whether an image x_i is a real image of its domain \mathcal{X}_i or a fake image generated by G , i.e., $D_i(x_i) = D(x_i | d_i)$.

3.2. Aligned Disentangling Training

We detail the overall training scheme now. Fig. 4 shows an overview of our model training scheme which consists of domain translation training and domain discriminative training. Same- and cross-domain translations are operated in domain translation training to separate off responsibilities of encoder and decoder and establish the relationship between the domain labels and the transferring directions. In domain discriminative training, encoder and decoder are trained to fool a discriminator which in turn tries to differentiate between generated samples and real samples.

Since content representation c_1 and c_2 may not be aligned in the shared content space \mathcal{C} , which may deteriorate the lossy transformation problem, we further propose a training algorithm to align disentangling representation in the shared space. This algorithm contains two portions: 1) the decoder is only trained during the auto-encoder training; and 2) the discriminator is trained to distinguish between the auto-encoding reconstructed images and generated images. Since G_D is just trained during the auto-encoder training, it can only decode the $c_i \in \mathcal{C}$ conditioned on the corresponding domain label d_i , which can be treated as a static content reconstruction function during cross-domain translation. As a consequence, the encoder is optimized to fool the discriminator by aligning c_i and c_j in the latent space, so that c_j ($j \neq i$) can be decoded conditioned on d_i for the cross-domain translation.

3.3. Further Interpretation

We present more insight about the proposed AD-GAN. In unpaired image-to-image translation, the exact global properties in the image domain \mathcal{X}_1 (e.g., nuclei size and amount) are not accessible without ground truth, while the global properties are required to synthesize mask domain \mathcal{X}_2 ; this could result in the content inconsistency between image domain \mathcal{X}_1 and mask domain \mathcal{X}_2 . On the other hand, generating the mask domain with ellipse/ellipsoid simulations could be too simple to reflect the real nuclei shapes, which also leads to content inconsistency when learning cross-domain translations. This is the main challenge in the current unpaired image-to-image translation. To better explain, we show an additional illustration in Fig. 5 where each domain \mathcal{X}_1 or \mathcal{X}_2 contains three parts: 1) domain-invariant content features C^I , i.e. the content consistency, 2) domain-specific content features C^S , i.e. the content inconsistency caused by different distribution, size, and/or number of nuclei of two unpaired domains 3) styles (S). *Ideally, we should map C_1^I with C_2^I , retain C_S without translating C_1^S and C_2^S , and disentangle S from C .*

Recent disentangled representation methods e.g. MUNIT and DRIT could well learn domain-invariant content features, i.e. C_1^I and C_2^I . Unfortunately, it does not constrain the styles and assumes style features sit in a space (see Fig. 2b), which cannot reflect the inherit nature of nuclei cell images. A too flexible style space would lead that domain-specific content features C^S will be considered as styles. Moreover, disentangled methods destyle the input images firstly, and then sample a new style to generate cross-domain images. Consequently, C^S would be lost during unpaired image translation, resulting in the well-known lossy transformation problem. This can be seen in Fig. 5 (a) where MUNIT aligns C_1^I and C_2^I only while considering both S_1, S_2 and C_1^S, C_2^S as styles.

In comparison, AD-GAN makes two major contributions: 1) *a within-domain single style is assumed* that typically holds in nuclei cell images. Thus, only S_1 and S_2 are considered as styles and disentangled. This alleviates the macro-level lossy transformation problem by preserving content explicitly, but they may translate $\{C_1^S, C_1^I\}$ with $\{C_2^S, C_2^I\}$ (see Fig. 5 (b)). This still leads to problems, since C_1^S and C_2^S are domain-specific content and should not be translated. 2) *We further propose the novel ADT algorithm* that promotes to align C_1^I with C_2^I , but retain C_1^S (or C_2^S) in the other domain (see Fig. 5 (c)). As such, the micro-level lossy transformation problem can be well solved. These contributions lead to substantial performance improvement over the present methods such as MUNIT.

3.4. Overall Loss

A one-to-one mapping between the images x_i and the corresponding content representations c_i can be built

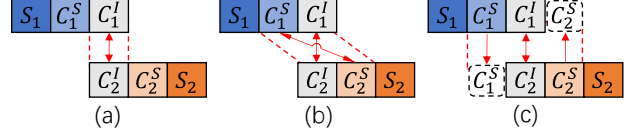


Figure 5. Illustration of content and style translation in (a) Disentangled methods, (b) AD-GAN w/o ADT and (c) AD-GAN.

through training an auto-encoder. This can be achieved by the same-domain translation with the image reconstruction loss, which ensures that the generator can reconstruct the original image within a domain. The image reconstruction loss is shown as follows:

$$\mathcal{L}_{rec}(G_E, G_D) = \mathbb{E}_{x_i \sim p(x_i)} [\|G_D(G_E(x_i, d_i), d_i) - x_i\|_1]. \quad (1)$$

GAN is typically used in order to build a one-to-one mapping between $c \in \mathcal{C}$ and two image domains \mathcal{X}_1 and \mathcal{X}_2 in unsupervised content and style disentanglement [14, 21, 22]. Unlike the standard adversarial training where discriminator distinguish between real and fake images, our discriminator only sees the images reconstructed by the frozen decoder G_D^* . The adversarial loss is shown as follows:

$$\mathcal{L}_{adv}(G_D, D) = \mathbb{E}_{c_i \in \mathcal{C}} [\log D(G_D^*(c_i, d_i) | d_i)] + \mathbb{E}_{c_j \in \mathcal{C}} [1 - \log D(G_D^*(c_j, d_i) | d_i)], \quad (2)$$

where \mathcal{C} is the encoded representation by G_E , $i \neq j$. Here under the aligned disentangling training, since G_D^* is a conditional content reconstruction function, the discriminator D is actually trained to distinguish from c_i and c_j . As a consequence, c_i and c_j shall be aligned by the generator on semantic object level to ensure c_j can be decoded conditioned on d_i to fool the discriminator.

We also exploit the content reconstruction loss during cross-domain translation that proves still useful even after we apply the aligned disentangling training. This loss is shown as follows:

$$\mathcal{L}_{ctr}(G_E, G_D) = \mathbb{E}_{c_i} [\|G_E(G_D^*(c_i, d_j), d_j) - c_i\|_1]. \quad (3)$$

Moreover, we utilize the cycle consistency loss proposed in CycleGAN [32]. When a given input x_1 passes through the cross-domain translation pipeline $\mathcal{X}_1 \rightarrow \mathcal{X}_2 \rightarrow \mathcal{X}_1$, it should be able to be reconstructed back to x_1 itself. The cycle consistency loss is shown as follows:

$$\mathcal{L}_{cyc}(G_E, G_D) = \mathbb{E}_{x_i \in p(x_i)} [\|G_D^*(G_E(G_D^*(G_E(x_i, d_i), d_j), d_j), d_i) - x_i\|_1]. \quad (4)$$

Finally, we jointly train the encoder, decoder, and domain discriminator to optimize the full objective:

$$\arg \min_{G_E, G_D} \arg \max_D \mathcal{L}_{adv} + \lambda_{cyc} \mathcal{L}_{cyc} + \lambda_{rec} \mathcal{L}_{rec} + \lambda_{ctr} \mathcal{L}_{ctr},$$

	Methods	Fluo-N2DL-HeLa			HaCaT		
		Precision	Recall	DICE	Precision	Recall	DICE
Unsupervised	CycleGAN	74.3 \pm 10.2	70.6 \pm 11.8	72.2 \pm 10.3	75.2 \pm 13.7	58.3 \pm 16.0	63.6 \pm 13.7
	MUNIT	81.8 \pm 12.7	63.5 \pm 9.9	71.2 \pm 11.0	78.4 \pm 8.1	54.6 \pm 16.3	61.6 \pm 12.7
	UDCT	85.2 \pm 3.5	82.4 \pm 3.8	83.7 \pm 3.3	77.1 \pm 9.6	66.1 \pm 10.5	69.5 \pm 8.81
	CGU-net*	72.3 \pm 2.1	79.6 \pm 2.6	75.7 \pm 0.9	83.6 \pm 0.4	66.8 \pm 0.7	73.5 \pm 0.4
	AD-GAN	92.8\pm1.0	89.2\pm1.4	90.9\pm0.6	85.4\pm0.5	95.2\pm0.1	89.3\pm0.2
Supervised	U-Net [†]	88.4 \pm 2.1	93.9 \pm 0.8	91.0 \pm 1.4	89.1 \pm 3.3	93.2 \pm 3.2	90.5 \pm 0.8
	nnU-Net [†]	97.1 \pm 0.3	83.1 \pm 0.2	89.1 \pm 0.2	87.8 \pm 0.4	98.2 \pm 0.2	92.7 \pm 0.3

Table 1. Quantitative comparison on 2D data. Here [†] indicates a supervised segmentation model and * indicates a two-stage model trained with paired synthetic data.

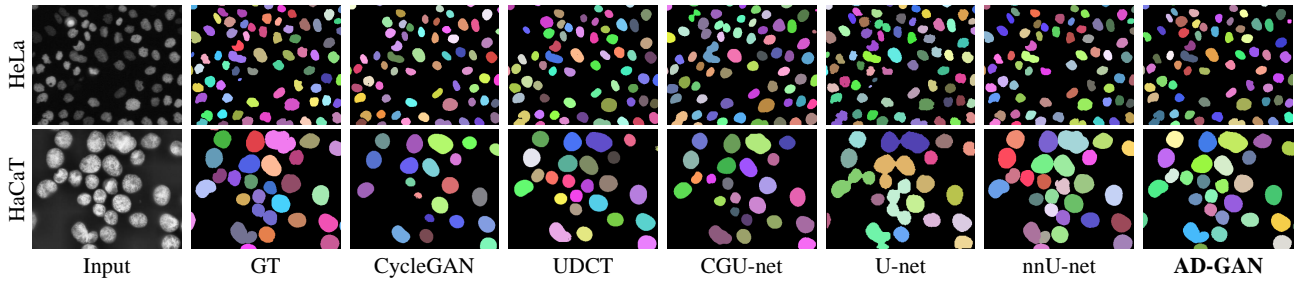


Figure 6. Visualization of test results on 2D data Fluo-N2DL-HeLa and HaCaT.

where each term is respectively described in Eqns. 1-4, and λ_{cyc} , λ_{rec} , λ_{ctr} are the trade-off parameters to adjust the importance of each term.

4. Experiments

4.1. Setup

Network Architecture We follow [14] and adopt the its architecture for our generative networks. For the generator used in AD-GAN, the encoder consists of 2 down-sampling residual blocks and 4 standard residual blocks, while the decoder exploits 4 conditional residual blocks and 2 up-sampling residual blocks, which all equipped with AdaIN [13]. The discriminator was designed based on PatchGAN [17], which contains LeakyReLU for nonlinearity.

Training Strategy We follow the setting in CycleGAN [32] and use LSGANs [25] to stabilize the training. In all the experiments, we tune the weight λ_{ctr} , λ_{cyc} and λ_{rec} empirically. The ADAM solver [18] is used with a batch size of 16. All the networks are trained from scratch with a learning rate of 0.0001 and weight decay 0.0001. The learning rate remains unchanged for the first 100 epochs and is linearly decayed to zero over the next 100 epochs.

4.2. Datasets

Fluo-N2DL-HeLa is a 2D benchmark set from the cell tracking challenge [27], containing 2 sequences of labelled and 2 sequences of unlabeled images. For unsupervised models, we use all images without any labels for training.

HaCaT is 2D dataset collected from a recently published dataset S-BSST265 [19]. It contains 26 training images and 15 testing images with different magnification, which are scaled to the same magnification (20 \times).

BBBC024 is a 3D dataset [7] containing 80 simulated HL60 cell nuclei images with different degree of clustering collected from Board Bioimage Benchmark Collection.

Scaffold-A549 is a 3D fluorescence microscope dataset for A549 cell culture on bio-scaffold, which contains 20 unlabelled images for training and one image was fully annotated for quantitative measurement.

4.3. Results on 2D Datasets

We first compare our method with competitive models in unsupervised nuclei segmentation on two 2D benchmark datasets. In particular, CGU-net [2] and UDCT [31] are two latest methods which probably obtain the best performance so far in 2D unsupervised nuclei segmentation task. We also select CycleGAN [32] and MUNIT [14], two most representative general-purpose unpaired image-to-image translation under different assumptions (see Fig. 2).

Following the previous research, we take the pixel-based metric to evaluate the performance. Specifically, we report precision, recall, and DICE coefficient [26] to evaluate different approaches. Here $\text{DICE} = \frac{2 \times n_{TP}}{n_{TP} + n_{FP} + n_{FN}}$, where n_{TP} , n_{FP} , n_{FN} are defined to be the number of true-positives, false-positives and false-negative segmentation result pixels in an image, respectively. A higher DICE coefficient indicates a better intersection between the ground

truth and the predicted segmentation masks.

We train each method for five times and report the means and standard deviation for quantitative evaluations. The comparison results are shown in Table 1. As observed, our proposed AD-GAN achieves significantly higher performance in both precision and DICE than all the unsupervised models on both the 2D datasets. More specifically, AD-GAN attains 90.9% and 89.3% on Fluo-N2DL-HeLa and HacaT respectively, which improve relatively the best of the other models by 8.3% and 21.5%. In addition, it is noted that CycleGAN, MUNIT and UDCT generate a much larger standard deviation compared with that of AD-GAN. On the other hand, although CGU-net enjoys a low standard deviation as well, its performance highly depends on the quality of synthetic data. Stable performance presents one appealing feature of our AD-GAN model.

To further examine the AD-GAN’s performance, we even compare it with two famous supervised models, i.e. U-Net [30] and nnU-Net [15]. nnU-Net is one of the state-of-the-art supervised semantic segmentation method on many biomedical data, which is a standardize baseline with no need for the manual intervention. As seen in the bottom part of Table 1, despite its unsupervised nature, AD-GAN can surprisingly lead to very similar performance to the supervised models. Without expensive manual annotations, the unsupervised AD-GAN model has a great potential to be applied in practice.

Finally, we engage a simple post-processing containing morphological erosion and 2D watershed to visualize the segmentation results. We illustrate in Fig. 6 one example for each of the two 2D dataset respectively. As clearly observed, those CycleGAN based methods, i.e. the standard CycleGAN, UDCT, CGU-net, typically lead to the lossy transformation problem, *e.g.* nuclei offset, nuclei deletion or addition. In comparison, our proposed AD-GAN can reduce such negative effects significantly and shows much better performance among all the unsupervised models.

4.4. Results on 3D Datasets

We now evaluate the various models on the more challenging 3D data for unsupervised nuclei segmentation. For fair comparison, we follow SpCycleGAN [10] and use the original CycleGAN as the baseline to synthesize the image masks. To adapt to 3D image-to-image translation task, we replace the 2D convolution layer with the 3D convolution layer and decrease the dimension of each layer to half for memory saving. We use the typical voxel-based metric to compare our method AD-GAN with the existing competitive models in unsupervised 3D nuclei segmentation including the original CycleGAN [32], SpCycleGAN [10], and the DeepSynth [8]. Particularly, DeepSynth is widely recognized as the state-of-the-art deep model for unsupervised 3D nuclei segmentation. We also evaluate our model

Methods	Precision	Recall	DICE
BBBC024			
CellProfiler	81.3	91.0	85.9
ImageJ Squash	76.1	99.5	86.2
CycleGAN	94.0	63.4	75.8
SpCycleGAN	76.4	71.1	73.7
DeepSynth *	63.4	66.6	64.9
AD-GAN	93.8	91.5	92.6
Scaffold-A549			
CellProfiler	37.5	91.3	53.1
ImageJ Squash	51.7	78.6	62.3
CycleGAN	53.9	41.7	47.0
SpCycleGAN	52.3	47.7	49.7
DeepSynth *	49.9	42.3	45.8
AD-GAN	89.0	78.2	83.3

Table 2. Comparison on 3D data BBBC024 and Scaffold-A549.

* indicates a two-stage model trained with paired synthetic data.

against the famous biomedical image processing tools Cell-Profiler 3.0 [6] and Squash [29].

The voxel-based segmentation results are again evaluated quantitatively based on precision, recall and DICE. These results are reported in Table 2. As observed on both 3D datasets, biomedical image processing tools tend to over-segment the images, which results in a high recall but low precision. On BBBC024 dataset which contains relatively simple data, CycleGAN based methods can obtain encouraging results. However, a position offset and shape difference problem can still be observed in the experiments. In comparison, our proposed AD-GAN shows the very promising result of 92.6%, which is much higher than all the other models. Meanwhile, Scaffold-A549 is a more challenging dataset where cells tend to grow on the scaffold, making the object distribution non-uniform and highly complicated. Uneven distribution of nuclei in 3D images makes the lossy transformation problem even worse. Therefore, a large content inconsistency would exist between the real image data and synthetic mask data. All the other comparison models perform very poor on this dataset. In contrast, our proposed AD-GAN fully utilizes the advantages of the end-to-end training and obtains 83.3% on Scaffold-A549 w.r.t. DICE, which is substantially higher than the best of the comparison models, achieved by Squash. More visualization are provided in the supplementary document.

4.5. Ablation Study

To analyze the importance of different components in our model, we conduct an ablation study with five variants of AD-GAN, as shown in Table 3. The ablation study on three components suggests that \mathcal{L}_{rec} , \mathcal{L}_{ctr} and \mathcal{L}_{cyc} suggest that the reconstruction on image-level and feature-level are important to establish correspondence between content and

Same-domain image reconstruction \mathcal{L}_{rec}	-	✓	✓	✓	✓	✓
Cross-domain content reconstruction \mathcal{L}_{ctr}	✓	-	✓	✓	✓	✓
Cycle Consistency \mathcal{L}_{cyc}	✓	✓	-	✓	✓	✓
AdaIN in Encoder	✓	✓	✓	-	✓	✓
Aligned disentanglin training	-	-	-	-	-	✓
Fluo-N2DL-HeLa	87.9	85.1	64.4	88.0	89.1	91.1
HaCaT	78.9	78.7	49.2	79.6	80.2	89.3
BBBC024	76.5	75.8	58.0	79.2	80.6	92.6
Scaffold-A549	75.6	73.2	52.4	78.3	80.2	83.3

Table 3. Ablation study of AD-GAN. Note that on Fluo-N2DL-HeLa, the performance is measured on both the sequences.

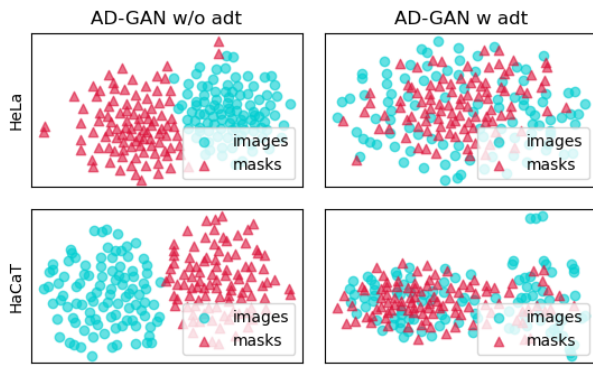


Figure 7. Visualization of content representations of two domains using t-SNE [20]. adt denotes aligned disentanglin training.

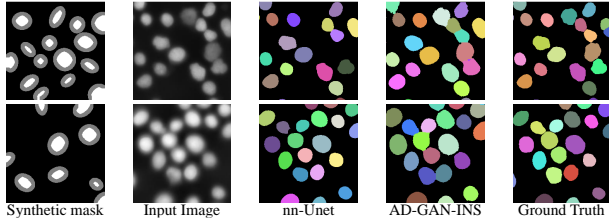


Figure 8. Visualization of instance segmentation results on HaCaT.

style. Once built, it is observed that the macro-level lossy transformation problem have been alleviated by preserving content explicitly during cross-domain translation. We also find that adding AdaIN in the encoder also helps improve the performance, since introducing domain information determines the translation direction. Finally, when we implement the aligned disentanglin training, AD-GAN can enforce the disentangled content for each domain to be well aligned in the latent space as visualized in Fig. 7. This consequently benefits largely the content preserving and helps reduce the micro-level lossy transformation problem.

4.6. Instance Segmentation

By better coping with the lossy transformation problem, our method can be readily extended to instance segmentation. Without modifying other settings, we exploit the gray

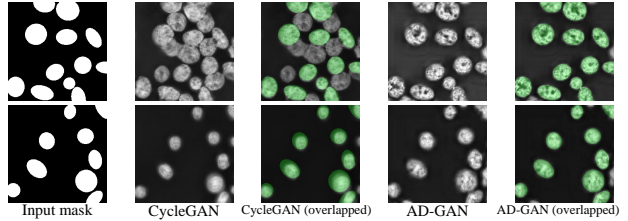


Figure 9. Visualization of image synthesis results on HaCaT.

color to represent the edge of each object and use them to generate the mask domain. Such results are shown in the first column of Fig. 8. Once such a model is trained (called as AD-GAN-INS), the instance segmentation can be obtained easily with a threshold and marker-based watershed algorithm, as shown in the fourth column of Fig. 8. Compared with the AD-GAN semantic segmentation outputs, clustered nuclei can be separated efficiently. Particularly, on HaCaT we got the object-based F1-Score (0.5 IoU threshold) of 95.2%, which is competitive when compared with 97.3% obtained by the supervised method nnUnet. More results can be seen in the supplementary document.

4.7. Image Synthesis

Although our method can output instance segmentation end-to-end in an unsupervised manner, it is required in more complex tasks, *e.g.* cell tracking, to generate or synthesize training data. In such case, the performance of generating cell images from synthetic masks is also essential. We demonstrate that AD-GAN could lead to much better performance than the standard CycleGAN when generating cell images from the mask domain in Fig. 9. To better visualize the difference (or highlight the lossy transformation problem in CycleGAN), we also show the input masks and generated images together in one single image (see the 3rd and 5th column of Fig. 9). As observed, without any shape difference and position offset, our method can generate more real images.

5. Conclusion

In this paper, we propose the Aligned Disentangling Generative Adversarial Network (AD-GAN) for end-to-end unsupervised nuclei segmentation. AD-GAN takes advantages of disentangled representation under within-domain same-style assumption to reduce macro-level lossy transformation problem. We further propose a novel training strategy to align the disentangled content representation in the hidden space in order to release micro-level lossy transformation problem. Our proposed method can be readily extended to instance segmentation tasks and image synthesis directly. Compared with existing deep-learning based unsupervised nuclei segmentation methods, AD-GAN demonstrates significantly better performance on both 2D and 3D data.

References

[1] Amjad Almahairi, Sai Rajeswar, Alessandro Sordoni, Philip Bachman, and Aaron C. Courville. Augmented cyclegan: Learning many-to-many mappings from unpaired data. In *International Conference on Machine Learning*, 2018. 3

[2] Moritz Bohland, Tim Scherr, Andreas Bartschat, Ralf Mikut, and Markus Reischl. Influence of synthetic label image object properties on gan supported segmentation pipelines. *Computational Intelligence Workshop*, 2019. 2, 6

[3] Nicolas Brieu, Armin Meier, Ansh Kapil, Ralf Schoenmeyer, Christos G. Gavriel, Peter D. Caie, and G'nter Schmidt. Domain adaptation-based augmentation for weakly supervised nuclei detection. *arXiv preprint arXiv:1907.04681*, 2019. 2

[4] Yunjey Choi, Youngjung Uh, Jaejun Yoo, and Jung-Woo Ha. StarGAN v2: Diverse image synthesis for multiple domains. In *IEEE Conf. Comput. Vis. Pattern Recog.*, 2020. 4

[5] Casey Chu, Andrey Zhmoginov, and Mark Sandler. Cyclegan, a master of steganography. *arXiv preprint arXiv:1712.02950*, 2017. 2

[6] Mc Quin Claire, Goodman Allen, Chernyshev Vasiliy, Kamentsky Lee, Beth A. Cimini, Kyle W. Karhohs, Doan Minh, Liya Ding, Susanne M. Rafelski, and Thirstrup Derek. Cell-profiler 3.0: Next-generation image processing for biology. *Plos Biology*, 16(7):e2005970–, 2018. 7

[7] Svoboda David, Kozubek Michal, and Stejskal Stanislav. Generation of digital phantoms of cell nuclei and simulation of image formation in 3d image cytometry. *Cytometry Part A*, 75A(6):494–509, 2009. 6

[8] Kenneth W. Dunn, Chichen Fu, David Joon Ho, Soonam Lee, Shuo Han, Paul Salama, and Edward J. Delp. Deep-synth: Three-dimensional nuclear segmentation of biological images using neural networks trained with synthetic data. *Nature Scientific Reports*, 9(1):18295, 2019. 2, 7

[9] Thorsten Falk, Dominic Mai, Robert Bensch, Özgürn Çiçek, Ahmed Abdulkadir, Yassine Marrakchi, Anton Böhm, Jan Deubner, Zoe Jäckel, Katharina Seiwald, Alexander Dovzhenko, Olaf Tietz, Cristina Dal Bosco, Sean Walsh, Deniz Saltukoglu, Tuan Leng Tay, Marco Prinz, Klaus Palme, Matias Simons, Ilka Diester, Thomas Brox, and Olaf Ronneberger. U-net: deep learning for cell counting, detection, and morphometry. *Nature Methods*, 16(1):67–70, 2019. 1

[10] Chichen Fu, Soonam Lee, David Joon Ho, Shuo Han, Paul Salama, Kenneth W. Dunn, and Edward J. Delp. Three dimensional fluorescence microscopy image synthesis and segmentation. In *IEEE Conf. Comput. Vis. Pattern Recog. Worksh.*, pages 2302–2310, 2018. 2, 3, 7

[11] David Joon Ho, Chichen Fu, Paul Salama, Kenneth W. Dunn, and Edward J. Delp. Nuclei segmentation of fluorescence microscopy images using three dimensional convolutional neural networks. In *IEEE Conf. Comput. Vis. Pattern Recog. Worksh.*, pages 834–842, 2017. 2

[12] Le Hou, Ayush Agarwal, Dimitris Samaras, Tahsin M. Kurc, Rajarsi R. Gupta, and Joel H. Saltz. Robust histopathology image analysis: To label or to synthesize? In *IEEE Conf. Comput. Vis. Pattern Recog.*, 2019. 2

[13] Xun Huang and Serge Belongie. Arbitrary style transfer in real-time with adaptive instance normalization. In *Int. Conf. Comput. Vis.*, pages 1510–1519, 2017. 4, 6

[14] Xun Huang, Ming-Yu Liu, Serge Belongie, and Jan Kautz. Multimodal unsupervised image-to-image translation. In *Eur. Conf. Comput. Vis.*, 2018. 2, 3, 4, 5, 6

[15] Fabian Isensee, Paul F. Jäger, Simon A. A. Kohl, Jens Petersen, and Klaus H. Maier-Hein. Automated design of deep learning methods for biomedical image segmentation. *arXiv preprint arXiv:1904.08128*, 2020. 7

[16] Phillip Isola, Jun-Yan Zhu, Tinghui Zhou, and Alexei A Efros. Image-to-image translation with conditional adversarial networks. In *IEEE Conf. Comput. Vis. Pattern Recog.*, 2017. 4

[17] Phillip Isola, Jun-Yan Zhu, Tinghui Zhou, and Alexei A. Efros. Image-to-image translation with conditional adversarial networks. In *IEEE Conf. Comput. Vis. Pattern Recog.*, 2017. 6

[18] Diederik P. Kingma and Jimmy Ba. Adam: A method for stochastic optimization. *arXiv preprint arXiv:1412.6980*, 2014. 6

[19] F. Kromp. An annotated fluorescence image dataset for training nuclear segmentation methods, 2019. 6

[20] Van Der Maaten Laurens and Geoffrey Hinton. Visualizing data using t-sne. *Journal of Machine Learning Research*, 9(2605):2579–2605, 2008. 8

[21] Hsin-Ying Lee, Hung-Yu Tseng, Jia-Bin Huang, Maneesh Kumar Singh, and Ming-Hsuan Yang. Diverse image-to-image translation via disentangled representations. In *Eur. Conf. Comput. Vis.*, 2018. 2, 3, 5

[22] Hsin-Ying Lee, Hung-Yu Tseng, Qi Mao, Jia-Bin Huang, Yu-Ding Lu, Maneesh Kumar Singh, and Ming-Hsuan Yang. Drit++: Diverse image-to-image translation via disentangled representations. *Int. J. Comput. Vis.*, pages 1–16, 2020. 2, 3, 5

[23] Alexander H. Liu, Yen-Cheng Liu, Yu-Ying Yeh, and Yu-Chiang Frank Wang. A unified feature disentangler for multi-domain image translation and manipulation. In *Adv. Neural Inform. Process. Syst.*, 2018. 3

- [24] Quan Liu, Isabella M. Gaeta, Bryan Millis, Matthew J. Tyska, and Yuankai Huo. Gan based unsupervised segmentation: should we match the exact number of objects. In *Image Processing*, 2021. [2](#)
- [25] Xudong Mao, Qing Li, Haoran Xie, Raymond Y. K. Lau, Zhen Wang, and Stephen Paul Smolley. Least squares generative adversarial networks. In *Int. Conf. Comput. Vis.*, 2017. [6](#)
- [26] F. Milletari, N. Navab, and S. Ahmadi. V-net: Fully convolutional neural networks for volumetric medical image segmentation. In *2016 Fourth International Conference on 3D Vision (3DV)*, pages 565–571, 2016. [6](#)
- [27] Beate Neumann, Thomas Walter, Jean-Karim Hériché, Jutta Bulkescher, Holger Erfle, Christian Conrad, Phill Rogers, Ina Poser, Michael Held, Urban Liebel, Cihan Cetin, Frank Sieckmann, Gregoire Pau, Rolf Kabbe, Annelie Wünsche, Venkata Satagopam, Michael H. A. Schmitz, Catherine Chapuis, Daniel W. Gerlich, Reinhard Schneider, Roland Eils, Wolfgang Huber, Jan-Michael Peters, Anthony A. Hyman, Richard Durbin, Rainer Pepperkok, and Jan Ellenberg. Phenotypic profiling of the human genome by time-lapse microscopy reveals cell division genes. *Nature*, 464(7289):721–727, 2010. [6](#)
- [28] Xingchao Peng, Zijun Huang, Ximeng Sun, and Kate Saenko. Domain agnostic learning with disentangled representations. In *Proceedings of Machine Learning Research*, 2019. [3](#)
- [29] A. et al Rizk. Segmentation and quantification of subcellular structures in fluorescence microscopy images using squassh. *Nature Protocols*, 9:586–596, 2014. [7](#)
- [30] O. Ronneberger, P. Fischer, and T. Brox. U-net: Convolutional networks for biomedical image segmentation. In *Medical Image Computing and Computer-Assisted Intervention*, volume 9351, pages 234–241, 2015. [7](#)
- [31] Ihle Stephan, Andreas Reichmuth, Sophie Girardin, Hana Han, Flurin Stauffer, Anne Bonnin, Marco Stampanoni, Janos Voros, and Csaba Forro. Udct: Unsupervised data to content transformation with histogram-matching cycle-consistent generative adversarial networks. *Nature Machine Intelligence*, 2019. [2, 3, 6](#)
- [32] Jun-Yan Zhu, Taesung Park, Phillip Isola, and Alexei A Efros. Unpaired image-to-image translation using cycle-consistent adversarial networks. In *Int. Conf. Comput. Vis.*, 2017. [2, 5, 6, 7](#)